Conf 9109118 -21

LA-UR 91-3169

LA-UR--91-3169

DE92 002413

Los Alamos National Laboratory is operated by the University of California for the United States Department of Energy under contract W-7405-ENG-36.

TITLE: INEX SIMULATIONS OF THE OPTICAL PERFORMANCE OF THE AFEL

AUTHOR(S): J. C. Goldstein, T. S. F. Wang, and R. L. Sheffield

SUBMITTED TO: Nuclear Instruments and Methods in Physics Research, Proceedings of the 13th International Free-Electron Laser Conference, Santa Fe, New Mexico, August 25-30, 1991

DISCLAIMER

MASTER

Los Alamos Los Alamos National Laboratory
Los Alamos, New Mexico 87545

FORM NO 836 R4
ST NO 2629 5/81

INEX Simulations of the Optical Performance of the AFEL*

John C. Goldstein, Tai-Sen F. Wang, and Richard L. Sheffield

Group X-1, MS F645

Los Alamos National Laboratory

Los Alamos, New Mexico 87545

(505) - 667 - 7281

(505) - 665 - 3389 (FAX)

ABSTRACT

The AFEL (Advanced Free-Electron Laser) Project at Los Alamos National Laboratory is presently under construction. The project's goal is to produce a very high-brightness electron beam which will be generated by a photocathode injector and a 20 MeV rf-linac. Initial laser experiments will be performed with a 1-cm-period permanent magnet wiggler which will generate intense optical radiation near a wavelength of 3.7 μm. Future experiments will operate with "slotted-tube" electromagnetic wigglers (formerly called "pulsed-wire" wigglers). Experiments at both fundamental and higher-harmonic wavelengths are planned. This paper presents results of INEX (Integrated Numerical EXperiment) simulations of the optical performance of the AFEL. These simulations use the electron micropulse produced by the accelerator/beam transport code PARMELA in the 3-D FEL simulation code FELEX.

1.0 Introduction.

The AFEL Project of the Los Alamos National Laboratory is intended to demonstrate that a very high-brightness electron beam can be generated in a relatively compact system by using a third-generation photocathode/rf-linac. The electron beam will first be used in a relatively conservative FEL oscillator (which is the primary topic of this paper) which will operate at an optical wavelength of about 3.7 μm using a permanent magnet wiggler with a 1-cm period. Further details of the design and expected performance of the accelerator can be found in [1]. The beam transport system from the end of the linac through the wiggler to the beam dump is discussed in detail in [2]. The extremely high brightness of the electron beam requires a new type of wiggler to fully exploit this characteristic for FEL oscillator operation. Such a new class of wigglers, previously called "pulsed-wire wigglers" but now renamed "slotted-tube wigglers" to more accurately reflect their construction, has been suggested by R. W. Warren and is discussed by him in [3].

In this work, we shall present a schematic layout of the experimental components of the AFEL and leave a detailed discussion of each one to the above-mentioned papers [1] - [3]. We then shall

*Work performed under the auspices of the U. S. Department of Energy and funded by a Los Alamos Special Supporting Research Initiative.

discuss the characteristics of the electron beam micropulse generated from PARMELA simulations of the photocathode/linac/beam transport system. Following the characterization of the calculated electron beam properties, we shall present the characteristics of the permanent magnet wiggler and the optical resonator which will be used in 3.7 μm operation.

The theoretical method used to study some of the expected characteristics of the AFEL is the INEX (Integrated Numerical EXperiment) method [4]. This method uses the results of numerical simulations of the photocathode/rf-linac/beam transport system, done with the code PARMELA, in the 3-D finite-pulse FEL simulation code FELEX [5]. The term INEX is generally understood to include 1-D simulations as well [6], [7], since as yet not all FEL physics is treatable with a single code.

The primary results of this paper will then be presented: (a) small-signal gain from 3-D finite-pulse multipass simulations; (b) saturated-gain steady-state oscillator output from 3-D finite-pulse multipass simulations; (c) effects of a misaligned electron beam; (d) effects of misaligned resonator mirrors; and, (e) cavity length detuning characteristics from 1-D finite-pulse simulations. We then briefly discuss the prospects of higher-harmonic operation at visible wavelengths with a short-period slotted-tube wiggler. Finally, we summarize our results and draw some conclusions.

2.0 Description of components of the AFEL.

2.1 Schematic layout of the device.

The AFEL is intended to be a very compact FEL. A schematic layout of the major components is shown in Figure 1. Note that the scale of the figure is set by the six-foot-tall figure shown standing next to the photocathode injector. All of the elements (except the beam dump) following the end of the linac are mounted on an optical table which itself is mounted in the vertical plane. The magnets used for the beam transport line are adjustable permanent magnets. Not shown in Figure 1 is the laser which drives the photocathode, and the 20 MW klystron which powers the rf-linac. Further details can be found in [1], [2], and [8].

2.2 Characteristics of the electron beam from PARMELA simulations.

The design of the photocathode injector/linac/beamline was done in [1] and [2] with the code PARMELA. The resulting electron micropulse at the entrance to the wiggler magnet has the characteristics shown in Figure 2. The mean energy of the beam is about 21.1 MeV ($\gamma_0 = 41.4$), the fractional energy spread $\Delta\gamma/\gamma_0 = 0.5$ %, and the "90%" normalized transverse emittances in the x- and y-directions are $\varepsilon_{nx} = \varepsilon_{ny} = 8\,\pi$ mm-mr. Here, the xz-plane is the plane of the electrons' wiggle motion in the undulator, and the yz-plane is the plane of betatron motion. The electron micropulse shape is almost "square" with a peak curent of about 175 A and a width of about 13.3 ps.

These characteristics are optimal in the sense that detrimental effects, such as misalignments, have not been included.

2.3 Parameters of the wiggler.

The wiggler for the first laser experiments will be made of permanent magnetic material ($SmCo_5$) with a remanent field of B_r = 8718.68 G. The design will be a Halbach two-block-per-period scheme. The blocks are 0.5 cm x 0.5 cm which leads to a wiggler period of λ_w = 1 cm. The wiggler field B_w (in Gauss) will thus depend on the (full) gap (in cm) as given by the expression B_w = 7,125.8 exp(-π(gap - 0.12705)). Table 1 shows other characteristics of the wiggler.

An important structural element will be an evacuated tube, 33.9725 cm long and 0.2 cm in diameter, centered at the center of the wiggler, through which the electron and optical beams will pass. The diameter of this tube, and the corresponding full gap of the wiggler, have been chosen to give the system tolerable optical vignetting losses and a sufficiently large small-signal gain to be comfortably above the threshold for laser action.

2.4 Parameters of the optical resonator.

The optical resonator will be a conventional two-mirror stable cavity. It will be mounted, along with elements of the electron beam transport system, on an optical table whose surface is oriented in the vertical plane. Some additional properties are given in Table 2. Note that the cavity loss is impacted by the beam tube through the wiggler. The performance results below use the mirror reflectivities given in Table 2 rather than values which would optimize the FEL output.

3.0 Results of numerical simulations of the performance of the AFEL.

3.1 Small-signal gain.

Using the electron micropulse from PARMELA, whose characteristics are shown in Figure 2, and the optical resonator whose properties are given in Table 2, we have calculated the self-consistent small-signal gain and optical pulse shape by doing a 3-D finite-pulse calculation with the FEL simulation code FELEX [5], [6], [7]. The calculation started from spontaneous emission noise and evolved until the optical pulse shape remained fixed from pass to pass but the amplitude grew at a constant rate. It was found that the net small-signal gain is about 42 % per pass; the empty-cavity loss due to vignetting by the beam tube and the 10 % outcoupling is 15.8 % at a wavelength of 3.3 μm. Figure 3a shows the evolution of the gain to a steady self-consistent value, and Figure 3b shows the small-signal power temporal profile of the optical pulse at steady-state. The peculiar optical pulse shape seems to be associated with small current fluctuations on the top of the current profile. Note that this result holds for a cavity length corresponding to exact synchronism.

3.2 Large-signal gain.

Figure 4 shows some features of the large-signal steady-state behavior from 3-D self-consistent INEX oscillator simulations. Figure 4a shows that the saturated gain through the wiggler is about 19 % at steady-state (corresponding to the total cavity loss of about 16 %). Figure 4b shows that the extraction efficiency reaches about 1.6 %, Figure 4c shows the distribution of electron energies at the end of the wiggler, and Figure 4d shows a profile of the optical pulse at the end of the wiggler. Note that the 3-D calculation does not have sufficient resolution to permit sidebands - those features are handled by 1-D simulations. Using an electron micropulse repetition frequency of 108 MHz and a macropulse duration of 10 μs, the laser should produce about 0.5 W of average output power at the repetition frequency of 1 Hz.

3.3 Effects of electron beam injection errors.

We have examined the effects on the magnitude of the small-signal gain of injecting the electron beam in the correct direction but displaced a small amount from the correct transverse position at the entrance to the wiggler. The optical resonator is assumed to be perfectly aligned with the axis of the wiggler. We have not used the full PARMELA electron micropulse in these calculations, but rather have done single-wavefront 3-D multipass simulations using the following electron beam characteristics: peak current I = 175 A, "90%" normalized transverse emitance $\varepsilon_n = 8\,\pi$ mm-mr, and a fractional energy spread (FW1/e) $\Delta\gamma/\gamma = 0.5$ %.

For perfect injection, the electron beam radius is about 0.015 cm; the minimum optical spot radius (w_0) is about 0.037 cm. The electron beam is focused in the x-direction to give a spot of circular transverse cross-section in the middle of the wiggler, while the beam is "matched" in the y-direction (the beam radius is constant along the length of the wiggler). An initial offset in y causes some betatron motion of the whole beam in the yz-plane. Table 3 shows results for the small-signal gain for various offsets.

3.4 Effects of mirror tilts.

We have examined the effects on the net small-signal gain of small tilts of the resonator mirrors. Multipass 3-D single-wavefront simulations were performed with the same electron beam parameters as in Section 3.3 (but the electron beam was assumed to be perfectly injected into the wiggler). In Table 4, the mirrors are identified as the downstream (d) or upstream (u) one relative to the direction of the electron velocity through the wiggler. Also shown in Table 4 are steady-state values of the net and gross small-signal gain.

3.5 Cavity length detuning properties.

We have investigated the cavity length detuning (desynchronism) characteristics of the AFEL using a 1-D time-dependent simulation code [6], [7]. The electron pulse was represented as a constant current for a total duration of 13.3 ps. Since emittance effects are not properly modeled in 1-D, it was necessary to reduce the curent to match the net small-signal gain from the 3-D finite-pulse INEX calculations.

Table 5 shows the steady-state optical power output as a function of the cavity length detuning δl relative to the case of exact synchronism ($\delta l = 0.0$). A positive value of δl indicates a cavity length longer than at exact synchronism; δl is measured in μm, and the total increase in optical path length due to a detuning δl is $2\delta l$.

3.6 Operation with a slotted-tube wiggler.

We have investigated the prospects for operation of the AFEL with a short-period, high-field pulsed microwiggler [3]. With the expected electron beam characteristics, this would allow operation at visible and ultraviolet optical wavelengths if the FEL was operated on a higher harmonic rather than the fundamental resonance wavelength. We performed 3-D single-wavefront simulations with an electron beam with the same characteristics as in Section 3.3, namely I = 175 A, ε_n = 8 π mm-mr, and $\Delta\gamma/\gamma = 0.5$ %. All gain and power values below are therefore peak micropulse values.

We assumed a slotted-tube microwiggler with the following characteristics: period $\lambda_w = 0.3$ cm, length $L_w = 6.0$ cm, $N = L_w / \lambda_w = 20$, peak wiggler field amplitude $B_w = 5.0538$ T, dimensionless vector potential $a_w = \sqrt{2}$, and a full gap = 0.1 cm. A Rayleigh range of 3 cm was assumed; this produces spots very much smaller than the mirror dimensions. The large-signal data refers to a gain of 10 %; the quoted output powers in Table 6 are outside the resonator, assuming 10 % outcoupling.

4.0 Summary and conclusions.

We have studied some characteristics of the optical performance of the Advanced Free-Electron Laser, which is presently under construction at Los Alamos, by means of INEX calculations. The results of the present study differ quantitatively with those of our previous work [9] because it was decided to build a room-temperature linac after [9] had been completed. Since a 20 MW klystron is available for this device, the additional copper losses of a room-temperature accelerator (compared with those of a cryogenic copper linac) limits the current to one half of the value previously assumed. This obviously greatly impacts the calculated laser performance figures. Additionally, in the present study we operate the linac at an electron energy of about 21 MeV which is 38 % higher than that assumed in [9].

Our method of study has used 3-D finite-pulse FEL simulations with the code FELEX [5], [6], [7] in which we used the electron beam micropulse obtained from PARMELA simulations of the photocathode injector/linac/beam transport system [1], [2]. To study the effects of electron beam injection errors, mirror tilts, and operation on a higher harmonic with a slotted-tube pulsed microwiggler [3], we did single-wavefront calculations with a model electron beam whose properties are taken from the full PARMELA result. We also studied cavity length detuning phenomena with 1-D simulations.

If the calculated electron beam properties can be achieved in practice, operation of the AFEL at an optical wavelength $\lambda \approx 3.3$ μm with a $\lambda_w = 1$ cm permanent magnet wiggler will be straightforward since the anticipated beam emittance is only about 1/5 of the operating optical wavelength, and the fractional energy spread is about 1/4 of the value allowed without serious degradation of the gain. The optical alignment tolerances and the electron beam injection tolerances seem to be quite moderate.

Operation with a short-period slotted-tube pulsed microwiggler on a higher harmonic would make optical wavelengths in the range of 0.35 - 0.60 μm accessible (for the particular microwiggler characteristics treated). Of course, the gains on all other harmonics, including the fundamental, would have to be suppressed. We did not examine alignment tolerances for this kind of operation, but they are expected to be more stringent than those for infrared operation.

References.

1. R. L. Sheffield, M. J. Browman, B. E. Carlsten, and L. M. Young, "Physics Design of the High Brightness Linac for the Advanced Free-Electron Laser Initiative at Los Alamos," these proceedings.

2. T.-S. Wang, K. C. D. Chan, R. L. Sheffield, and W. L. Wilson, "Design of the E-Beam Transport Line for the AFEL," these proceedings.

3. R. W. Warren, "Progress with the Slotted-Tube Pulsed Microwiggler," these proceedings.

4. J. C. Goldstein, B. D. McVey, B. E. Carlsten, and L. E. Thode, "Integrated Numerical Modeling of Free-Electron Lasers," Nucl. Instr. and Meth. in Phys. Res. A285, pp. 192 - 196 (1989).

5. B. D. McVey, "Three-Dimensional Simulations of Free-Electron Laser Physics," Nucl. Instr. and Meth. in Phys. Res. A250, pp. 449 - 455 (1986).

6. B. D. McVey, J. C. Goldstein, R. L. Tokar, C. J. Elliott, S. J. Gitomer, M. J. Schmitt, and L. E. Thode, "Numerical Simulations of Free-Electron Laser Oscillators," Nucl. Instr. and Meth. in Phys. Res. A285, pp. 186 - 191 (1989).

7. J. C. Goldstein, B. D. McVey, R. L. Tokar, C. J. Elliott, M. J. Schmitt, B. E. Carlsten, and L. E. Thode, "Simulation Codes for Modeling Free-Electron Laser Oscillators," in *Modeling and Simulation of Laser Systems,* Donald L. Bullock, Editor, Proc. SPIE 1045, pp. 28 - 35 (1989).

8. K. C. D. Chan, R. H. Kraus, J. Ledford, K. L. Meier, R. E. Meyer, D. Nguyen, R. L. Sheffield, F. L. Sigler, L. M. Young, T. S. Wang, W. L. Wilson, and R. L. Wood, "Los Alamos Advanced Free-Electron Laser," these proceedings.

9. J. C. Goldstein, R. L. Sheffield, B. E. Carlsten, and R. W. Warren, "Compact RF-Linac Free-

Electron Lasers," Nucl. Instr. and Meth. in Phys. Res. A296, pp. 282 - 287 (1990).

Figure Captions.

Figure 1. Schematic layout of the major components of the AFEL.

Figure 2a. Current vs. position within micropulse.

Figure 2b. Distribution in energy.

Figure 2c. Normalized emittance in x-direction vs. position.

Figure 2d. Normalized emittance in y-direction vs. position.

Figure 3a. Net small-signal gain vs. pass number.

Figure 3b. Steady-state self-consistent optical pulse shape.

Figure 4a. Gain through wiggler vs. pass number.

Figure 4b. Extraction efficiency vs. pass number

Figure 4c. Electron energy distribution after wiggler at steady-state.

Figure 4d. Optical power at the end of the wiggler at steady-state.

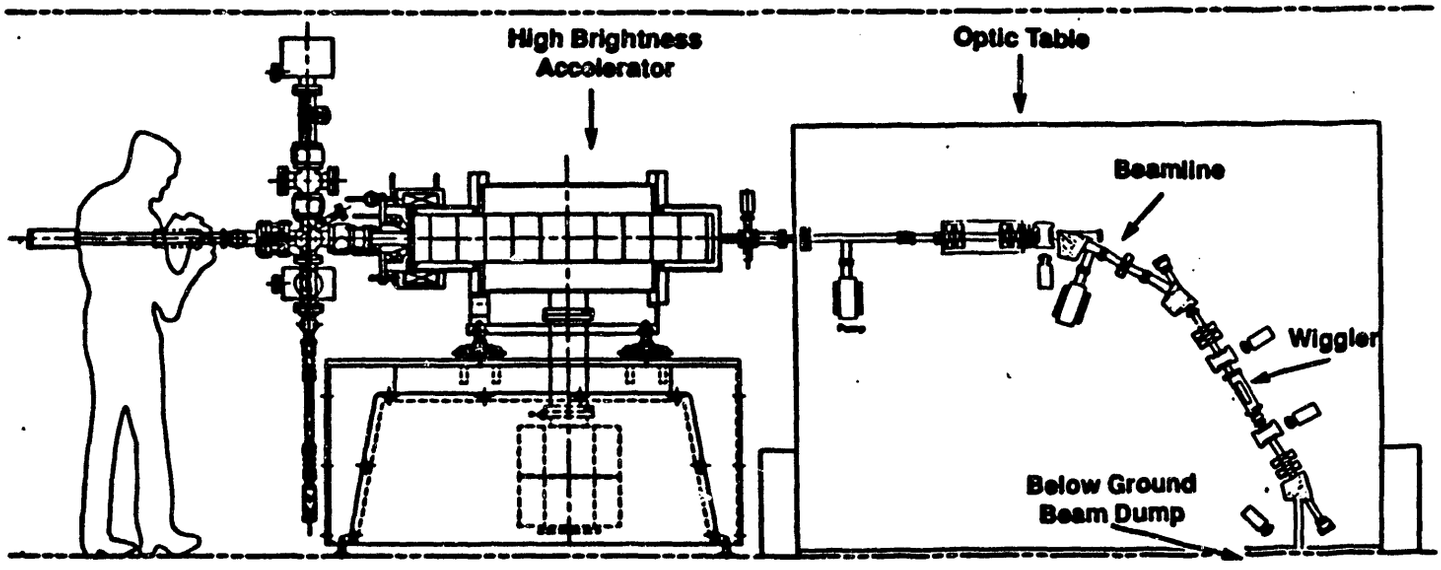

Figure 1. Schematic layout of the major components of the AFEL.

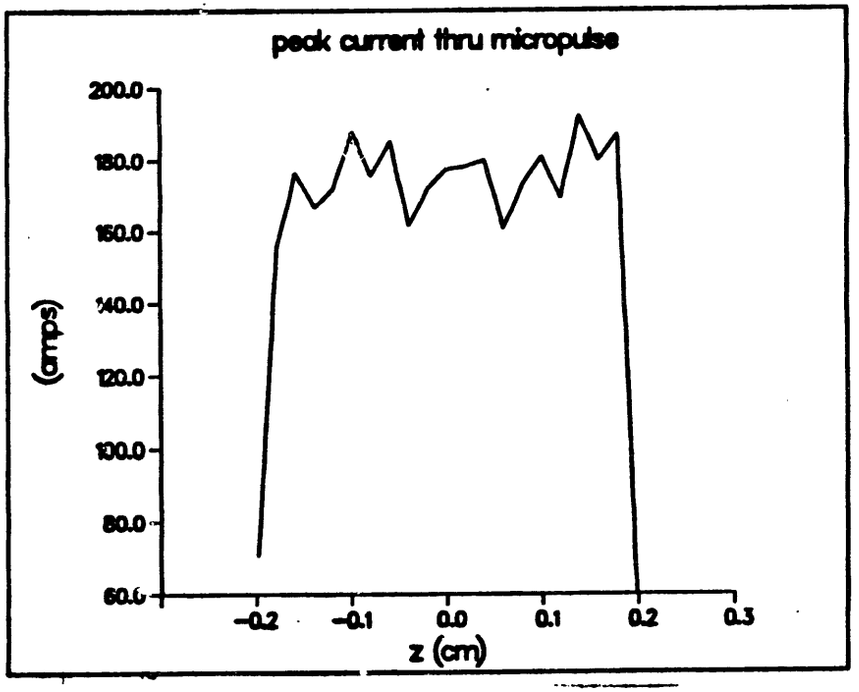

Figure 2a. Current vs. position within micropulse.

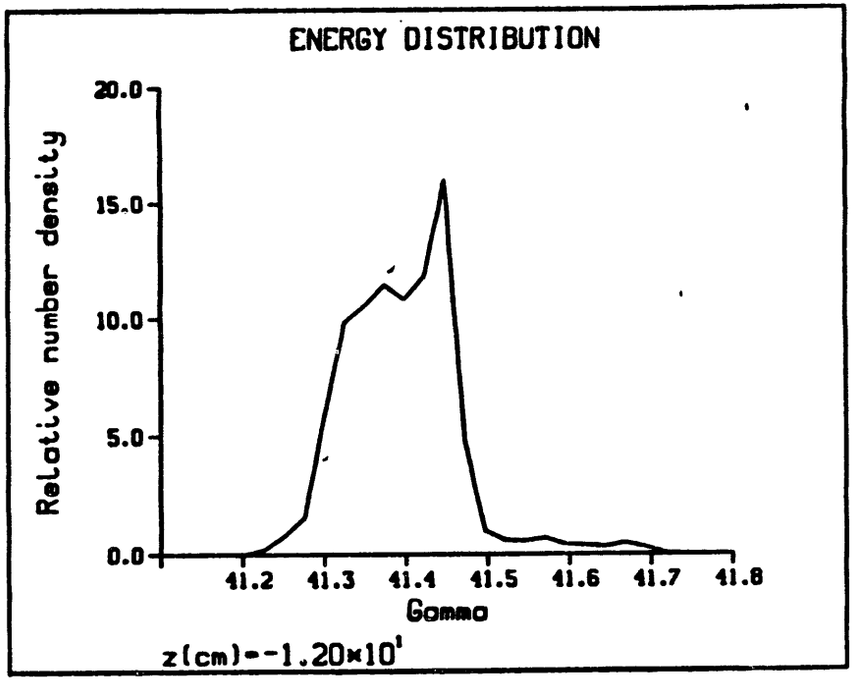

Figure 2b. Distribution in energy.

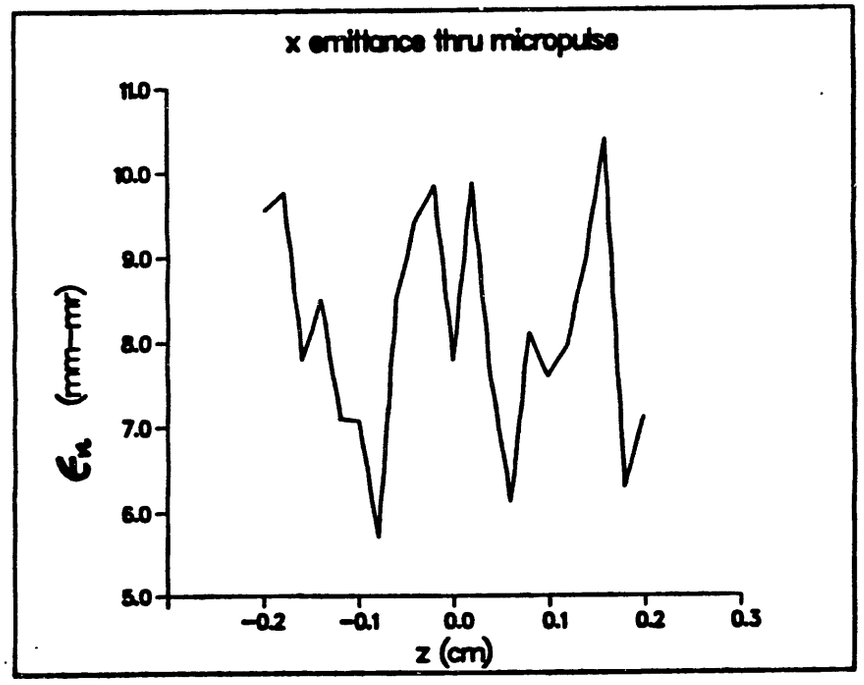

Figure 2c. Normalized emittance in x-direction vs. position.

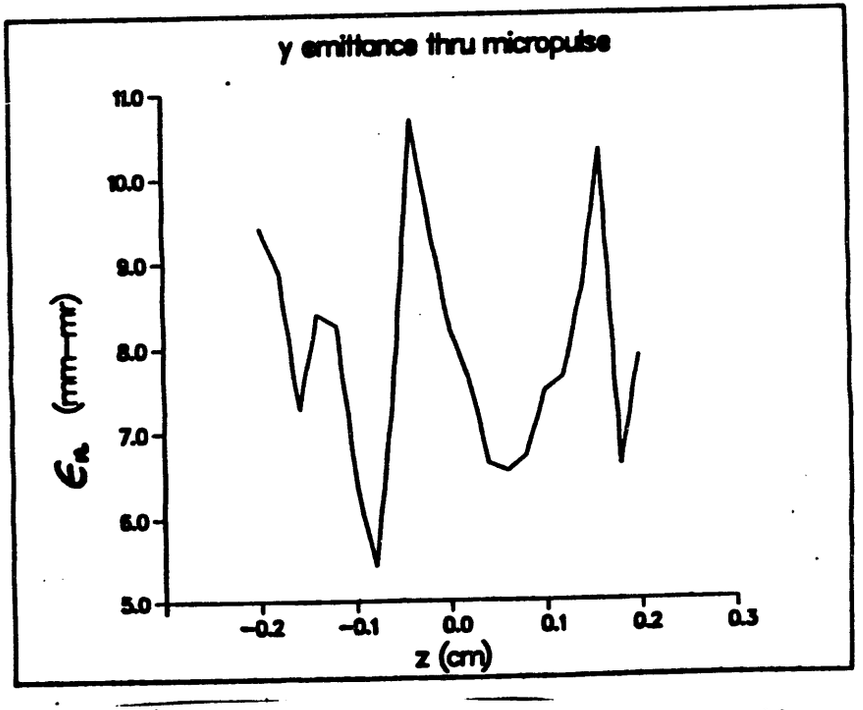

Figure 2d. Normalized emittance in y-direction vs. position.

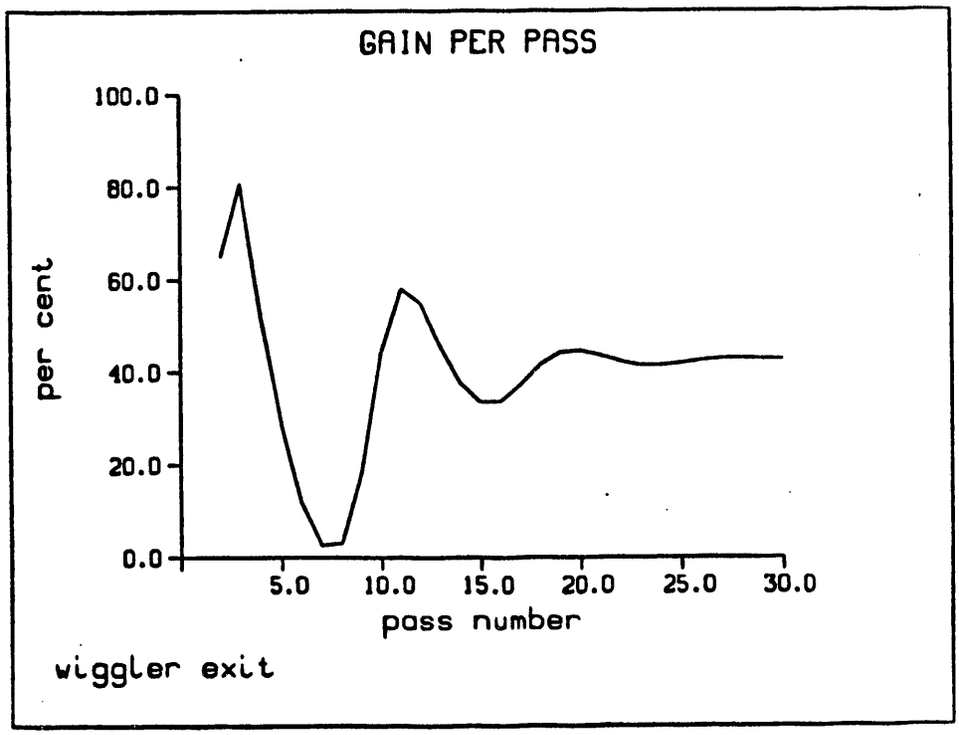

Figure 3a. Net small-signal gain vs. pass number.

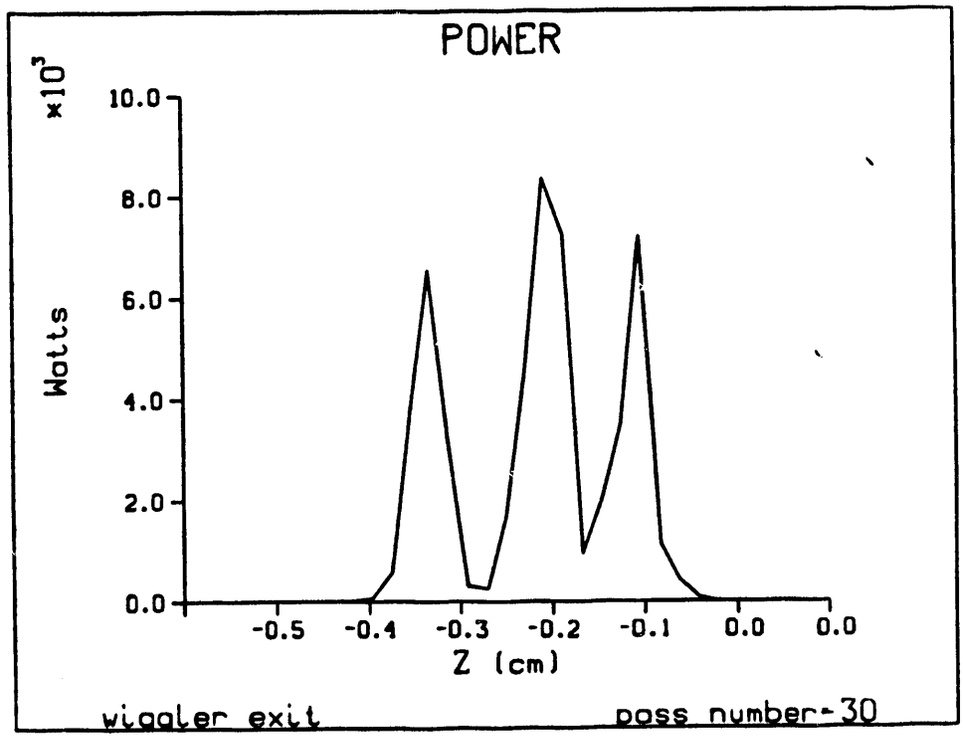

Figure 3b. Steady-state self-consistent optical pulse shape.

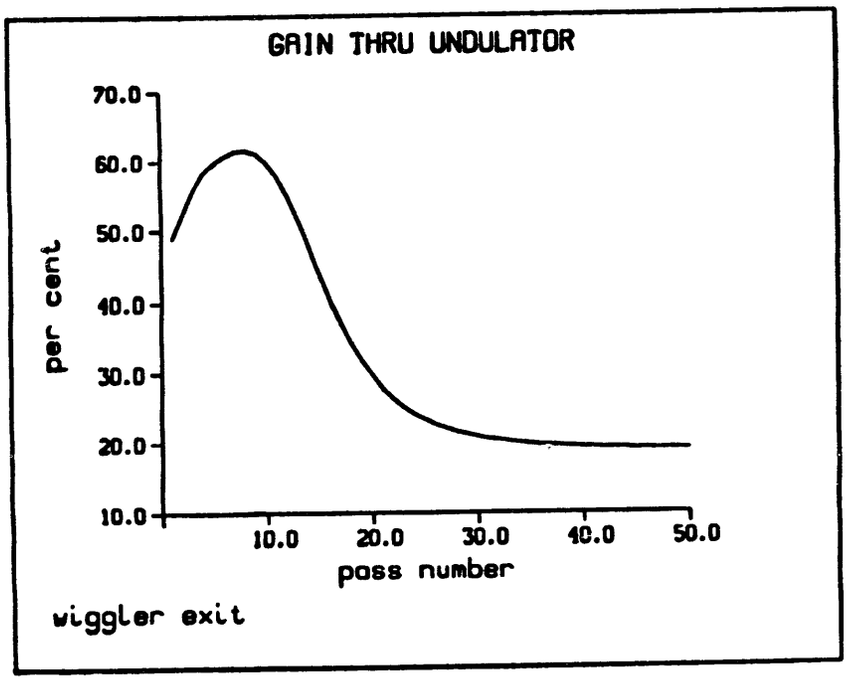

Figure 4a. Gain through wiggler vs. pass number.

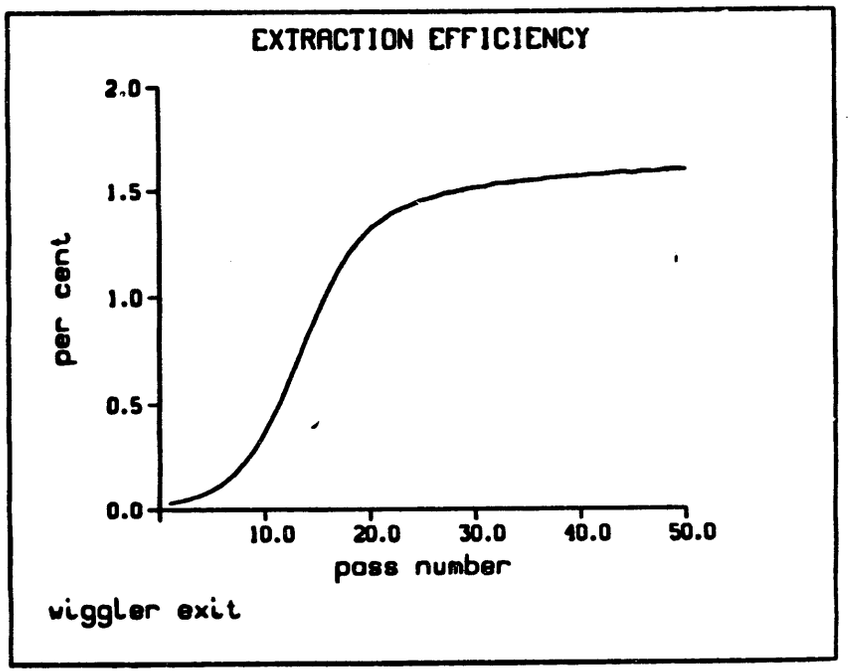

Figure 4b. Extraction efficiency vs. pass number

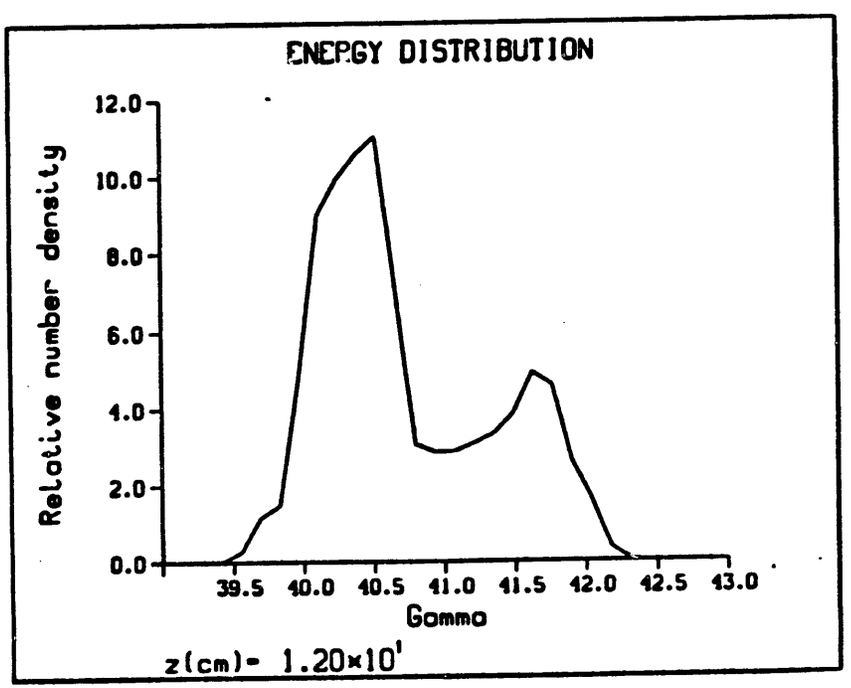

Figure 4c. Electron energy distribution after wiggler at steady-state.

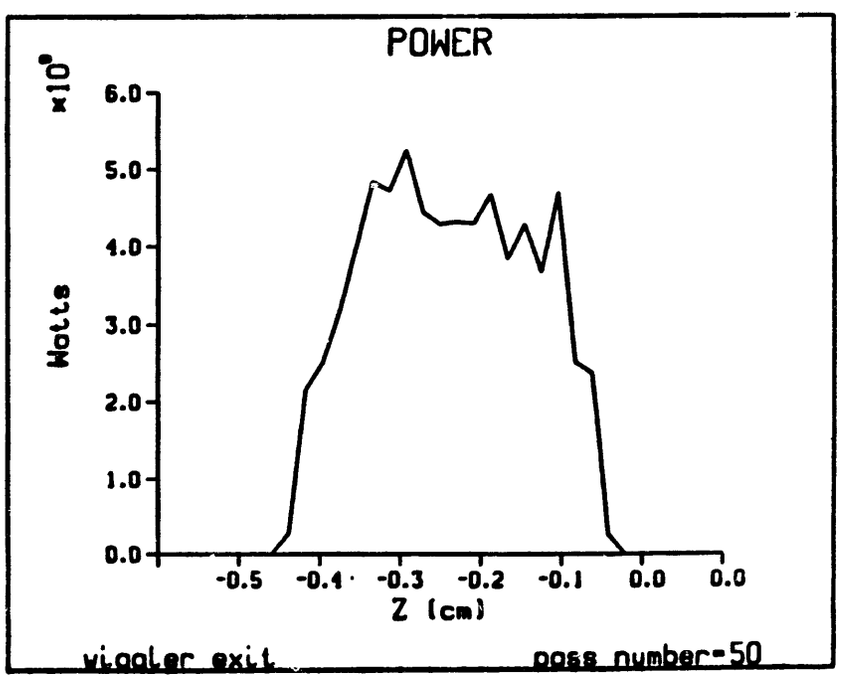

Figure 4d. Optical power at the end of the wiggler at steady-state.

Table 1: Parameters of the Permanent Magnet Wiggler

B_w (G)	4,842.632
full gap (cm)	0.25
a_w	0.451711
L_w (cm)	24.0
$N = L_w / \lambda_w$	24

Single-plane focusing

Table 2: Parameters of the Optical Resonator

length (cm)	138.46
Rayleigh range (cm)	10.0
location of focus of lowest mode	center of the wiggler
mirror radius (cm)	2.40
downstream mirror reflectivity	0.9
downstream mirror transmission	0.1
upstream mirror reflectivity	0.994
mirror composition	multilayer dielectrics

Table 3: Effects of Electron Beam Injection Errors

x-offset (cm)	y-offset (cm)	G_{ss} (gross,%)	G_{ss} (net,%)
0.0	0.0	70.6	45.2
0.01	0.01	55.4	31.0
0.02	0.02	28.0	7.0

Table 4: Effects of Mirror Tilts

tiltx (d, mr)	tilty (u, mr)	G_{ss} (gross,%)	G_{ss} (net,%)
+0.1	0.0	-30.0*	-30.0*
+0.1	0.0	55.0	20.0
+0.2	0.0	37.0	-24.0
+0.15	0.0	45.0	-1.8
+0.05	-0.05	62.0	32.0
+0.1	-0.1	43.7	2.4

*This is for an unloaded resonator. Recall that the aligned empty-cavity loss is 15.8 %.

Table 5: Cavity Length Detuning Characteristics

δl (μm)	relative steady-state power
-45.0	0.003
-35.0	0.096
-25.0	0.346
-15.0	0.564
0.0	1.000
+15.0	0.462
+25.0	0.123

Table 6: Performance with a Slotted-Tube Microwiggler

harmonic #	G_{ss} (%)	λ_{ss} (μm)	P_{out} (MW)	λ_{ls} (μm)
3.0	86.2	0.595	25.0	0.600
5.0	21.1	0.355	10.5	0.355

END

DATE FILMED

12/04/91